

Exploration of microscopic physical processes of Z-pinch by a modified electrostatic direct implicit particle-in-cell algorithm

Kaixuan Li(李开轩), Cheng Ning(宁成), Ye Dong(董烨), and Chuang Xue(薛创)

Citation: Chin. Phys. B, 2024, 33 (**9**): 095201. DOI: 10.1088/1674-1056/ad553a
Journal homepage: http://cpb.iphy.ac.cn; http://iopscience.iop.org/cpb

What follows is a list of articles you may be interested in

Scaling of rise time of drive current on development of magneto-Rayleigh-Taylor instabilities for single-shell Z-pinches

Xiaoguang Wang(王小光), Guanqiong Wang(王冠琼), Shunkai Sun(孙顺凯), Delong Xiao(肖德龙), Ning Ding(丁宁), Chongyang Mao(毛重阳), and Xiaojian Shu(束小建)
Chin. Phys. B, 2022, 31 (**2**): 025203. DOI: 10.1088/1674-1056/ac1fd9

Simulations on the multi-shell target ignition driven by radiation pulse in Z-pinch dynamic hohlraum

Shi-Jia Chen(陈诗佳), Yan-Yun Ma(马燕云), Fu-Yuan Wu(吴福源), Xiao-Hu Yang(杨晓虎), Yun Yuan(袁赟), Ye Cui(崔野), and Rafael Ramis
Chin. Phys. B, 2021, 30 (**11**): 115201. DOI: 10.1088/1674-1056/ac01c2

Numerical study on magneto-Rayleigh-Taylor instabilities for thin liner implosions on the primary test stand facility

Xiao-Guang Wang(王小光), Shun-Kai Sun(孙顺凯), De-Long Xiao(肖德龙), Guan-Qiong Wang(王冠琼), Yang Zhang(张扬), Shao-Tong Zhou(周少彤), Xiao-Dong Ren(任晓东), Qiang Xu(徐强), Xian-Bin Huang(黄显宾), Ning Ding(丁宁), Xiao-Jian Shu(束小建)
Chin. Phys. B, 2019, 28 (**3**): 035201. DOI: 10.1088/1674-1056/28/3/035201

Preliminary investigation on electrothermal instabilities in early phases of cylindrical foil implosions on primary test stand facility

Guanqiong Wang(王冠琼), Delong Xiao(肖德龙), Jiakun Dan(但家坤), Yang Zhang(张扬), Ning Ding(丁宁), Xianbin Huang(黄显宾), Xiaoguang Wang(王小光), Shunkai Sun(孙顺凯), Chuang Xue(薛创), Xiaojian Shu(束小建)
Chin. Phys. B, 2019, 28 (**2**): 025203. DOI: 10.1088/1674-1056/28/2/025203

Magneto-Rayleigh–Taylor instability in compressible Z-pinch liner plasmas

Xue Yang(杨学), De-Long Xiao(肖德龙), Ning Ding(丁宁), Jie Liu(刘杰)
Chin. Phys. B, 2017, 26 (**7**): 075202. DOI: 10.1088/1674-1056/26/7/075202

Exploration of microscopic physical processes of Z-pinch by a modified electrostatic direct implicit particle-in-cell algorithm

Kaixuan Li(李开轩), Cheng Ning(宁成)†, Ye Dong(董烨)‡, and Chuang Xue(薛创)

Institute of Applied Physics and Computational Mathematics, Beijing 100088, *China*

(Received 25 April 2024; revised manuscript received 26 May 2024; accepted manuscript online 7 June 2024)

For investigating efficiently the stagnation kinetic-process of Z-pinch, we develop a novel modified electrostatic implicit particle-in-cell algorithm in radial one-dimension for Z-pinch simulation in which a small-angle cumulative binary collision algorithm is used. In our algorithm, the electric field in z-direction is solved by a parallel electrode-plate model, the azimuthal magnetic field is obtained by Ampere's law, and the term for charged particle gyromotion is approximated by the cross product of the averaged velocity and magnetic field. In simulation results of 2 MA deuterium plasma shell Z-pinch, the mass-center implosion trajectory agrees generally with that obtained by one-dimensional MHD simulation, and the plasma current also closely aligns with the external current. The phase space diagrams and radial-velocity probability distributions of ions and electrons are obtained. The main kinetic characteristic of electron motion is thermal equilibrium and oscillation, which should be oscillated around the ions, while that of ion motion is implosion inwards. In the region of stagnation radius, the radial-velocity probability distribution of ions transits from the non-equilibrium to equilibrium state with the current increasing, while of electrons is basically the equilibrium state. When the initial ion density and current peak are not high enough, the ions may not reach their thermal equilibrium state through collisions even in its stagnation phase.

Keywords: Z-pinch, particle-in-cell, ion heating, charged particle collisions

PACS: 52.58.Lq, 52.65.Rr, 52.50.Sw, 52.20.Hv **DOI:** 10.1088/1674-1056/ad553a

1. Introduction

A cylindrical plasma with an axial current interacts with its self-generated magnetic field, giving rise to a radially inward $J \times B$ force on the plasma and triggering a self-contraction process, which is referred as Z-pinch. The Z-pinches have many significant applications in the field of high-energy density physics. The gas puff Z-pinch can be used as x-ray and neutron sources.[1–3] Wire-array Z-pinches can also be served as x-ray sources,[4,5] and a constructed load consists of wire arrays and foam columns can be employed to generate a dynamic hohlraum,[6–8] in which a capsule can be embedded for inertial confinement fusion.

During the run-in phase of Z-pinch process, the plasma is firstly accelerated towards the axis under $\boldsymbol{J} \times \boldsymbol{B}$ force. When enough charged particles of the plasma are driven to the axis, they get into the stagnation phase and then reach their maximal compression state. Subsequently, when the thermal pressure of the plasma exceeds the magnetic pressure, the plasma begins to expand (expansion phase). During the stagnation phase, the plasma emits intensively x-ray radiations and produces a large number of neutrons (for deuterium and tritium plasma) due to the extremely high density and temperature state. For radiation, ions transfer thermal energy to electrons, and electrons produce radiations through ionization, excitation and bremsstrahlung.[9] For neutron production, the ion temperature directly influences the yield of thermonuclear neutrons.[10] Therefore, the ion heating mechanism during the stagnation, even in the whole Z-pinch process is a significant issue for Z-pinch physical research.

In experiments, one can get the effective ion temperature from Doppler contributions to K lines.[11,12] However, there is still controversy regarding whether the effective ion temperature accurately reflects the actual ion thermal temperature.[13–15] According to the experimental results by Kroupp[16] *et al.*, the effective ion temperature includes large motion components, suggesting that the ion velocity probability distribution during the stagnation phase may be non-Maxwellian. Hence, the commonly used magnetohydrodynamic (MHD) models may be insufficient for analyzing ion heating mechanism during the stagnation phase. This is due to the fact that a fundamental assumption of MHD simulations is such that each fluid element is in thermal equilibrium. Moreover, in MHD simulations the ions are heated primarily by adiabatic compression (pdV work) rather than the ion kinetic energy directly thermalization.[17] The particle-in-cell (PIC) simulations, with a binary Monte Carlo algorithm for Coulomb collisions (MCC), can allow whether a plasma is in thermal equilibrium or non-equilibrium. Hence, the PIC simulations enable us to obtain the detailed physical images of the Z-pinch kinetic process.

Welch *et al.*[18] firstly simulated the Z-pinch process based on PIC simulation by using the LSP code. The LSP

†Corresponding author. E-mail: ning_cheng@iapcm.ac.cn

‡Corresponding author. E-mail: dong_ye@iapcm.ac.cn

© 2024 Chinese Physical Society and IOP Publishing Ltd

code employs a direct electromagnetic implicit PIC algorithm, and in recent years, the Chicago[19] code developed on the basis of LSP has incorporated an implicit magnetic field algorithm to further relax the constraints on the time step. Additionally, Angus *et al.*[20] proposed an energy-conserving PIC-MCC algorithm for Z-pinch simulation to address the numerical cooling issue that arises from the combination of implicit PIC and MCC algorithms. Both Welch's and Angus's schemes have relatively large computational costs in the solution of electromagnetic fields, which requires iterative methods for solving large sparse matrices. Moreover, existing researches using PIC method for Z-pinch simulations mostly focus on the neutron productions,[21–23] as the PIC method can originally distinguish between the productions of thermonuclear neutrons and beam-target neutrons. Therefore, we hope to establish a simpler PIC simulation model to study the physical processes during the stagnation phase of Z-pinch. Compared to the fluid simulation, it can accurately deal with the non-Maxwellian distributions of particle velocity, and compared to the published PIC methods using electromagnetic field solver, it is easier to implement and has a lower computational cost.

In this paper, we propose a modified electrostatic direct implicit PIC (ES-DI-PIC) method that threats the electric and magnetic fields separately, in radial one-dimensional space. The magnetic field is obtained from Ampere's law, neglecting the displacement current term, while the radial electric field is obtained through the solution of Poisson equation. Because of the decoupling of electric and magnetic fields, the computation of electric and magnetic fields becomes expedited. Section 2, the specific algorithms are presented, and in Section 3, some simulation results of Z-pinch stagnation process and their further discussion are provided, especially on the ion heating during the stagnation phase. Finally, some conclusions are reached in Section 4.

2. A modified ES-DI-PIC algorithm for Z-pinch radial 1D simulation

2.1. Axial current modeling and azimuthal magnetic-field calculation

In Z-pinch plasma, the axial current implies that the averaged velocities υ_z of electrons and ions in the axial direction are not equal to zero. To calculate the axial current, we decompose the z-direction velocity of a charged particle in Z-pinch plasma into two components: the directional velocity $\bar{\upsilon}_z$, representing the averaged axial velocity of particles, and the thermal velocity $\upsilon_z^{\rm th}$, which is a statistically averaged value of zero.

A parallel electrode-plate model is developed to calculate $\bar{\upsilon}_z$, in which the external current I flows into the anode, and the plasma current $I_{\rm p}$ flows out from the anode. The remaining charge Q on the anode is given by

$$Q^{n+1} = Q^n + (I^{n+1/2} - I_{\rm p}^{n+1/2})\Delta t, \tag{1}$$

where n is the time level, and Δt is the time interval for calculation. A uniform distribution of $\bar{\upsilon}_z$ for each species of particle is assumed in space for simplification of Z-pinch PIC calculation in radial one dimension. That would slightly cause more current and in turn magnetic field diffused into the interior of cylinder plasma, but it would not induce much changes overall in the particle kinetic motions due to the intense magnetic field and most charged particles distributed on the periphery of column. Since the current carried by electrons are much greater than that by ions, the current $I_{\rm p}$ carried with the plasma can be expressed as

$$\begin{aligned} I_{\rm p}^{n+1/2} &= \sum_j n_{{\rm e},j} q_{\rm e} \bar{\upsilon}_{z,{\rm e}}^{n+1/2} S_j + \sum_j n_{{\rm i},j} q_{\rm i} \bar{\upsilon}_{z,{\rm i}}^{n+1/2} S_j \\ &\approx \sum_j n_{{\rm e},j} q_{\rm e} \bar{\upsilon}_{z,{\rm e}}^{n+1/2} S_j, \end{aligned} \tag{2}$$

where $n_{{\rm e},j}$ and $n_{{\rm i},j}$ represent the electron density and ion density in the j-th radial grid, $q_{\rm e}$ and $q_{\rm i}$ are the electric charges of electron and ion, respectively, S_j represents the cross section of the j-th grid in the z-direction. In a typical Z-pinch load configuration, the diameter of the electrode plate is several times larger than the distance between cathode and anode, so the electric field in z-direction between the electrodes may be considered as one between the parallel electrode plate, i.e., $E_z = 4\pi Q/S_{\rm total}$, where $S_{\rm total}$ is the electrode plate area. By applying E_z, the particle directional velocity $\bar{\upsilon}_z$ can be obtained. The velocity advancing of particle can be expressed as

$$\bar{\upsilon}_z^{n+1/2} = \bar{\upsilon}_z^{n-1/2} + a_z^n \Delta t, \tag{3}$$

$$a_z^n = \frac{a_z^{n-1} + qE_z^{n+1}/m}{2}, \tag{4}$$

where a_z, m, and q represent the acceleration, mass, and charge of the particle, respectively. Combining Eqs. (1)–(4) yields

$$\begin{aligned} Q^{n+1} = Q^n + I^{n+1/2}\Delta t - \sum_j n_{{\rm e},j} q_{\rm e} \Delta t \left(\bar{\upsilon}_{z,{\rm e}}^{n-1/2} + \frac{a_{z,{\rm e}}^{n-1}\Delta t}{2} \right) S_j \\ - \frac{\sum_j 4\pi n_{{\rm e},j} q_{\rm e}^2 S_j \Delta t^2}{2mS_{\rm total}} Q^{n+1}. \end{aligned} \tag{5}$$

After obtaining Q^{n+1} through Eq. (5) and determining E_z through $E_z^{n+1} = 4\pi Q^{n+1}/S_{\rm total}$, then $\bar{\upsilon}_z$ at time level $n+1/2$ can be obtained through Eqs. (3) and (4). Subsequently, using Eq. (2), the plasma current $I_{\rm p}^{n+1/2}$ can be obtained. Lastly, since the contribution of displacement current to the magnetic field is estimated to be much smaller than that of conducting current in typical Z-pinch of hundred-ns driving current, and the displacement current may be neglected, which is also adopted the PIC simulations for laser-driven fast

ignition,[24,25] the azimuthal magnetic field can be calculated from Ampere's law as static magnetic field as follows:

$$B^n_{\theta,j+1/2} = \frac{\sum_{k=0}^{j}\left(I^{n+1/2}_{\mathrm{p},k} + I^{n-1/2}_{\mathrm{p},k}\right)}{4cr_{j+1/2}}, \tag{6}$$

where c is the light speed, and $r_{j+1/2}$ represents the position of grid $j+1/2$ in the radial direction.

2.2. Particle push scheme and radial electric-field calculation

The Z-pinch process can be reasonably described through pushing all charged particle movements inwards in self-consistent electromagnetic fields. Based on the electrostatic implicit particle-in-cell simulation algorithm[26] and the approximation of gyromotion of charged particle by averaged motion, the equation for particle motion in the radial direction in cylindrical Z-pinch can be expressed as

$$\upsilon_r^{n+1/2} = \upsilon_r^{n-1/2} + a_r^n\Delta t - \bar{\upsilon}_z^n B_\theta^n q\Delta t/mc, \tag{7}$$

$$a_r^n = (qE_r^{n+1}/m + a_r^{n-1})/2, \tag{8}$$

where υ_r and a_r are radial velocity and acceleration of charged particle, respectively, and E_r is the radial electric field felt by charged particle.

Compared to the particle motion equation in radial direction in standard electromagnetic direct implicit PIC algorithm,[27] in the third term on the right-hand side of Eq. (7) the particle velocity υ_z^n is replaced by the particle averaged velocity $\bar{\upsilon}_z^n$. The particle motion can be considered as the superposition of gyromotion and guiding center motion under the magnetic field. In Eq. (7), the use of $\bar{\upsilon}_z^n$ preserves the particle's guiding center motion while neglecting the gyromotion, which is similar to the $J_z \times B_\theta$ term appearing in the one-dimensional Z-pinch MHD fluid model. Similar to the direct implicit method,[26] the particle advance is divided into two steps. The first step of the particle motion is computed as

$$\upsilon_r^1 = \upsilon_r^{n-1/2} + a_r^{n-1}\Delta t/2, \tag{9}$$

$$r^1 = r^n + \upsilon_r^1\Delta t, \tag{10}$$

where r is the radial position of the particle. After obtained the particle position r^1 in the first step, the charge density ρ^1 can be determined by using the interpolation function. Here r^{n+1} is computed by

$$r^{n+1} = r^1 + \delta r, \tag{11}$$

$$\delta r = qE_r^{n+1}\Delta t^2/2m. \tag{12}$$

Using $\rho^{n+1} = \rho^1 + \delta\rho$ and $\delta\rho = -\nabla\cdot\boldsymbol{P} \approx -\nabla\cdot\rho^1\delta r$ (here $\boldsymbol{P}$ is called the dipole density[28]), we can obtain $\rho^{n+1} = \rho^1 - \nabla\cdot\delta r\rho^1$. By combining the Poisson equation and Eq. (12), the equation for the radial electric field at time level $n+1$ can be expressed as

$$\nabla\cdot(1+4\pi\chi)E_r^{n+1} = 4\pi\rho^1, \tag{13}$$

$$\chi = \frac{\rho^1 q\Delta t^2}{2m}. \tag{14}$$

After obtaining the solution E_r^{n+1} to Eq. (13), the particle second push can be performed, and its formula is

$$\upsilon_r^{n+1/2} = \upsilon_r^1 + qE_r^{n+1}\Delta t/2m - \bar{\upsilon}_z^n B_\theta^n q\Delta t/mc, \tag{15}$$

$$r^{n+1} = r^1 + (qE_r^{n+1}\Delta t/2m - \bar{\upsilon}_z^n B_\theta^n q\Delta t/mc)\Delta t. \tag{16}$$

The term $\bar{\upsilon}_z^n B_\theta^n q\Delta t/mc$ in the second push implies that the particle is pushed by the electrostatic field force and also by the Lorentz force in an averaged z-direction velocity. That decouples the electrostatic push and Lorentz force push of particle motion, and cannot be required to calculate the particle cyclotron motion in detail.

3. Simulation results and discussions

We simulated a deuterium plasma shell Z-pinch with a linear mass of 20 $\mu g\cdot cm^{-1}$. The function describing the variation of current with time is given by $I(t) = I_0\sin^4(2\pi t/4T_0)$, where the peak current is taken to be 2 MA, and current rise time T_0 from zero to peak is set to be 50 ns. The simulation starts after the driven current has flowed through into the Z-pinch plasma for 20 ns. The plasma configuration is considered as a hollow cylinder with inner radius of 0.6 cm and outer radius of 1.0 cm. At the initial moment of the simulation, deuterium ions and electrons are filled between the inner and outer radii in a uniform density of 3×10^{18} cm^{-3}. The temperature of both deuterium ions and electrons is 10 eV. The particle simulation region in the radial direction ranges from 0 to 1.5 cm, which is divided into 1500 cells, the averaged number of macroparticles per grid is about 600 and a time step of 0.2 ps is used. Coulomb collisions between particles are implemented by using Nanbu's small-angle cumulative binary collision algorithm.[29] The collisions of ion–ion, electron–electron, and electron–ion are fully considered. The computational collision time interval is set to be 10 times the time step of PIC simulation during the stagnation phase, while in other phases, it is set to be 100 times the time step.

3.1. The Z-pinch process

Figure 1 illustrates the obtained Z-pinch implosion trajectories of mass center by snow-plow, 1D MHD,[30,31] and PIC simulations, and those of main plasma inner and outer boundaries also by PIC simulation, as well their external and plasma current waveforms. In this study the main plasma is defined as the center 90% of total load mass. From Fig. 1, it can be found that the deuterium plasma shell expands first due to its higher

initial temperature, and the mass center implosion trajectory agrees roughly with the snowplow simulation's one, and better with the radial 1D MHD simulations' one, and also the Z-pinch plasma current calculated through Eq. (2) is almost the same as the external current set by a quartic sine function. This implies the simulation results by means of our novel Z-pinch PIC radial 1D algorithm presented above are physically reasonable overall, and in turn the algorithms are basically reasonable about the assumption of uniform distribution of $\bar{v}_z$ in radius, and the calculations of $\bar{v}_z$ and the static magnetic field, as well the approximation of gyromotion of charged particle in advance. Only a very small part of external current is held up on the electrode plates to form the axial electrostatic electric field. At around 60 ns, the Z-pinch plasma reaches its maximal compression state, and then expands.

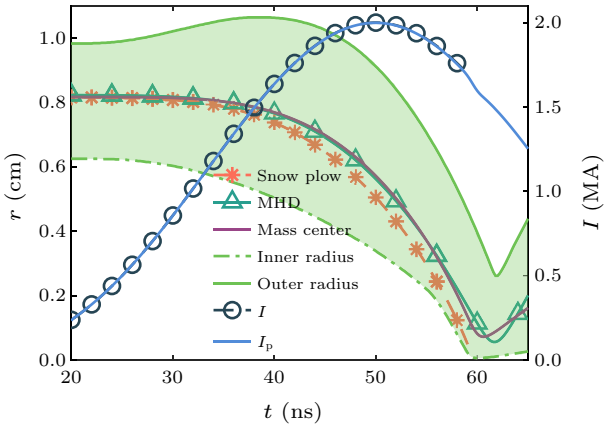


Fig. 1. The Z-pinch implosion trajectories of mass center obtained by snow-plow (dashed orange line with asterisk), 1D MHD simulation (solid green line with triangle), PIC simulation (solid purple line), and those of the inner (dash-dotted green line) and outer (solid green line) boundaries of main Z-pinch plasma obtained by PIC simulation. The variations of external (driven) current I (black line with hollow circles) and plasma current I_p (solid blue line) with time are also plotted here for showing the whole pinch process.

Figure 2 shows the spatiotemporal evolutions of ion density and temperature during the Z-pinch process. The ion temperature can be statistically calculated through this expression $T_i(\mathrm{eV}) = m_i \sum_{j=0}^{N_{\mathrm{icell}}} (v_{i,j} - \bar{v}_i)^2/(3N_{\mathrm{icell}}|q_e|)$, where m_i, $v_{i,j}$, and $\bar{v}_i$ are the mass, velocity, and averaged velocity of ions in a cell, N_{icell} is the ion number in a cell, $|q_e|$ is the absolute value of electron charge, and j is the particle number in order in a cell. During the run-in phase (before 59 ns), the plasma shell is compressed, and in turn the ion density and temperature increase. After 59 ns, the plasma enters into the stagnation phase, both the ion temperature and number density reach their maximal values, signifying that the ion thermal pressure has reached its maximum. Simultaneously, since the Z-pinch current is declining, the magnetic pressure tends to decrease. After 60 ns, one can observe a gradual decrease in ion density and temperature with the plasma shell expansion.[31] During the run-in phase, a small fraction of particles with higher velocity move into the inner vacuum region near the axis as seen in Fig. 2(a). Because the number of these particles in each cell may be relatively less, it may cause strong electric field fluctuations on the grid. Consequently, there are a small fraction of particles that reach the axis region prematurely.

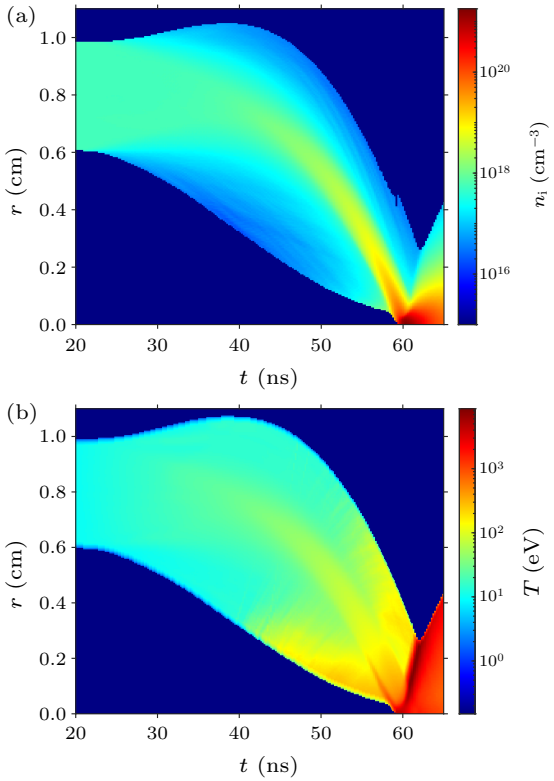


Fig. 2. Spatiotemporal evolutions of ion density (a) and ion temperature (b).

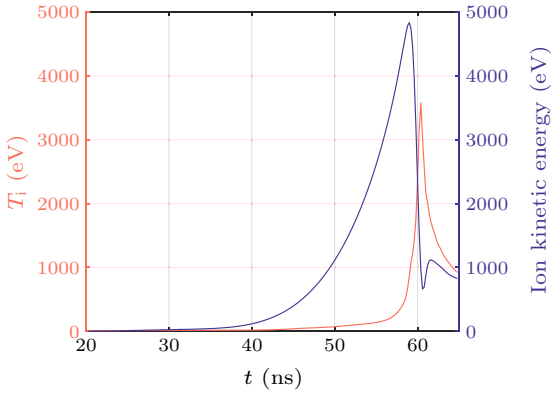


Fig. 3. Temporal variations of averaged ion kinetic energy and temperature.

3.2. The ion heating process

Figure 3 illustrates the variations of averaged ion kinetic energy and averaged ion temperature with time through statistics on particle velocities in our novel electrostatic PIC simulations. At the moment of a large number of plasma particles pinching to the axis, the averaged ion kinetic energy decreases sharply, and at the same time the averaged ion temperature rapidly increases. This indicates that the pinching plasma enters into stagnation at 59 ns. It is attributed to a large number

of particles moving inwards in all directions to get together, and inducing intensively Coulomb collisions and stagnation near the axis region, in which the kinetic energies of most ions are thermalized and some ions may be reflected into the opposite direction and movement outwards. When the ion kinetic energy increases again, the pinched plasma enters into expansion phase at 60.6 ns. This PIC simulated result is similar to the MHD calculated result of Z-pinch.

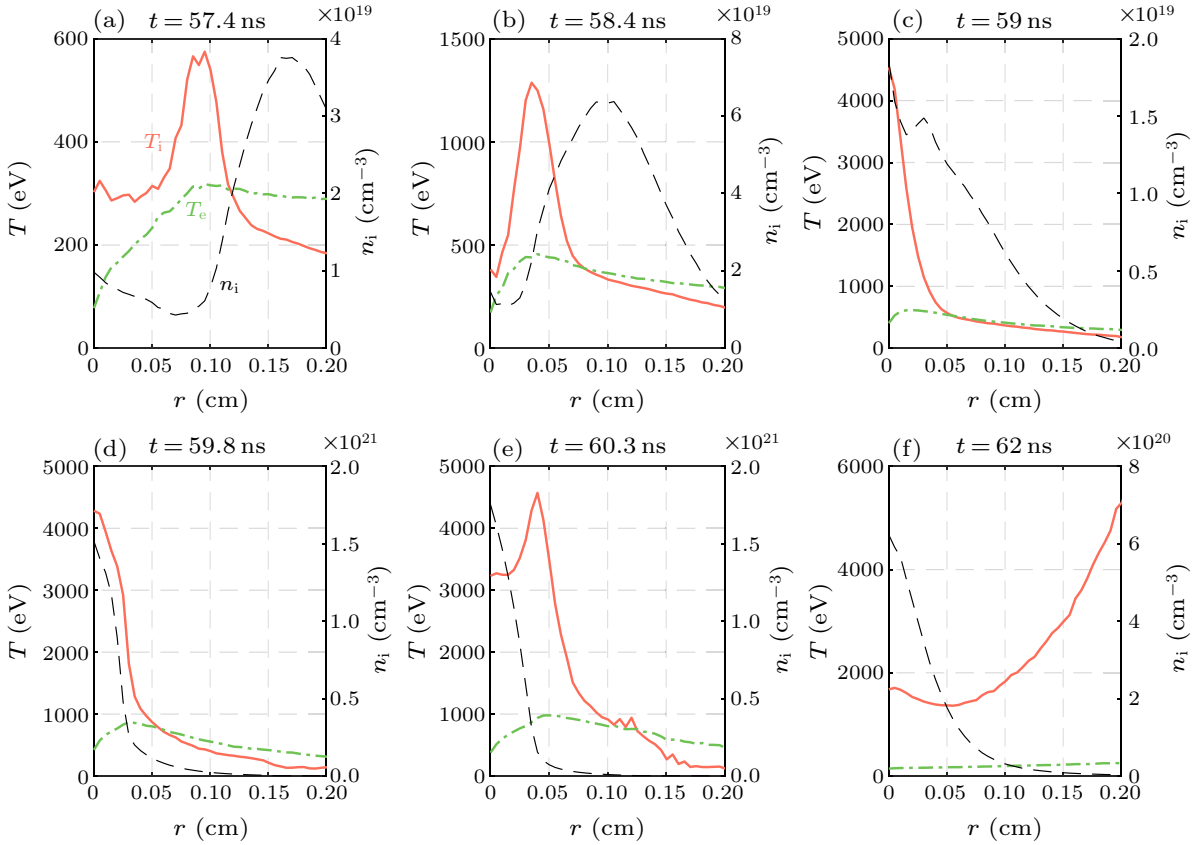


Fig. 4. Profiles of ion temperature (solid red line), electron temperature (short dashed green line), and ion density (long dashed black line) during the Z-pinch stagnation process, at 57.4 ns (a), 58.4 ns (b), 59.0 ns (c), 59.8 ns (d), 60.3 ns (e), and 62.0 ns (f).

Figures 4(a)–4(f) show the variations of ion temperature, electron temperature, and ion number density along the radius from 57.4 ns to 62 ns. Figure 4(c) ($t = 59$ ns) depicts the radial distributions of the variables at the start time of stagnation, and Fig. 4(e) ($t = 60.3$ ns) shows those at the maximal compression state. Figures 5(a)–5(f) are the diagrams of ion radial-velocity probability distributions in velocity–radius phase space at a few times corresponding to Figs. 4(a)–4(f), respectively. They exhibit clearly movements of all ion particles along radial directions and the stagnating and expanding processes in the particle system. As shown in Figs. 4(a) and 4(b), the ion temperature in the inner radius of plasma is higher than that in other place because the smaller ions existing in the front were disturbed and accelerated intensively through collision and pressure work. This ion heating mechanism might occur in many gas puff and wire-array Z-pinch experiments, because less precursor plasma or gas often already existed near the axis before the stagnation phase.[32] Figures 5(c)–5(e) illustrate the variable profiles during the stagnation phase, in which the particles are pinched to near the axis and its ion temperature increases to more than 4 keV. It can be found that the ion temperatures are much higher than the electron temperatures possibly due to the ion gained more energy there in collision. It should be noted that in Fig. 4(f), which illustrates the variable profiles in expansion, the temperatures of ion outside the main plasma seem too high possibly due to the ion non-Maxwellian distribution, and that they may be imprecise.

From Figs. 5(c)–5(e), it can be seen that more and more ion particles have been accumulated near the axis region. Specially in Fig. 5(e) ($t = 60.3$ ns), the ion averaged velocity looks like to be close to zero, and most of the ion particles stagnate together on the axis. The ion averaged velocity approaching to zero means that the ions are experiencing the thermalization process. However, the electrons carry relatively small kinetic energy, and the electron–ion relaxation time is calculated to be $\tau_{e,i} \geqslant 6$ ns (Ref. [33]) during stagnation phase, which is larger than the duration of stagnation phase (about 1.3 ns). Therefore, the ions and electrons should not reach an equilibrium state, and their temperatures are separated.

In Figs. 5(d) and 5(e), there are noticeable differences of

ion velocity probability distribution in different radial regions. On the side closer to the axis, ions' average velocity close to zero, while on the other side, ions have a significant drift velocity. Corresponding to Figs. 5(d) and 5(e), Fig. 6 illustrates the ion velocity probability distributions in different radial regions. In Fig. 6(a), in the region $r < 0.025$ cm, the ion velocity probability distribution approximates a Maxwellian distribution, indicating that these ions have already stagnated. The number of ions in this region is approximately 36% of the total number of ions. In the region 0.025 cm $< r <$ 0.2 cm, the ion velocity probability distribution exhibits significant drift velocities in the negative direction, indicating that these ions are still moving towards the axis. In Fig. 6(b), in the region $r < 0.04$ cm, the ion velocity probability distribution also approximates a Maxwellian distribution, with ions in this region increasing up to 69% of the total ion population. This suggests that the majority of ions have been stagnated. In the region 0.04 cm $< r <$ 0.2 cm, there are some ions moving along the positive direction, indicating that these ions are expanding outwards.

The primary influence on the azimuthal velocities of ion is exerted by Coulomb collisions. As shown in Fig. 7, the characteristics of ion thermal motion in the radial and azimuthal directions are similar. However, the azimuthal velocity of ions follows a Maxwellian distribution (as well as the axial velocity of ions), while the radial velocity exhibits a drift Maxwellian distribution.

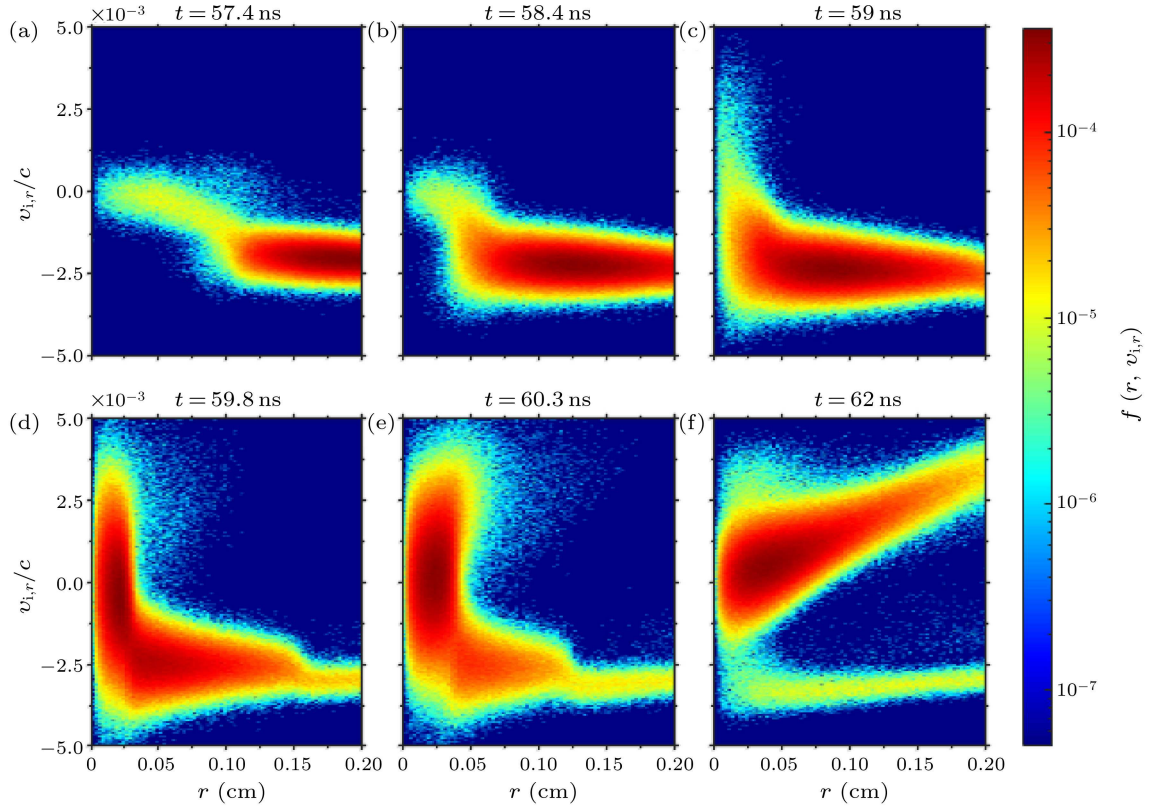


Fig. 5. Diagrams of ion radial-velocity probability distributions in phase space around the Z-pinch stagnation process, at 57.4 ns (a), 58.4 ns (b), 59.0 ns (c), 59.8 ns (d), 60.3 ns (e), and 62.0 ns (f).

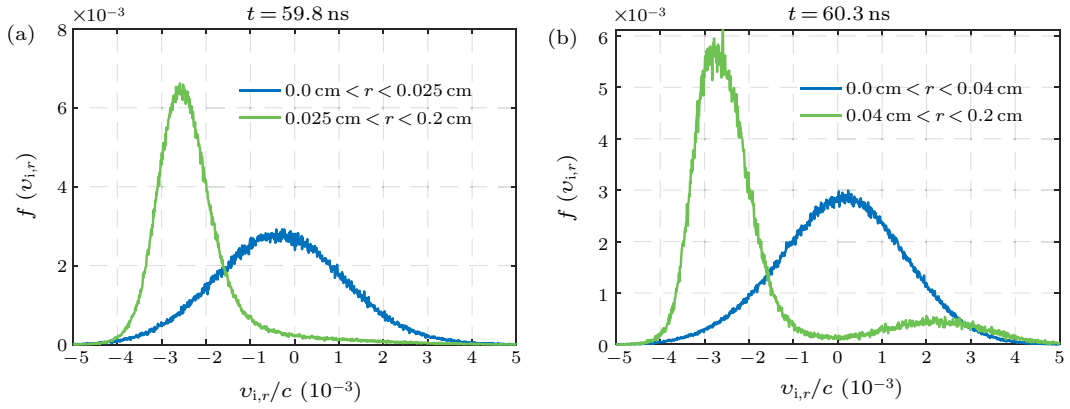


Fig. 6. Radial velocity probability distributions of ions in different radial regions at 59.8 ns (a) and 60.3 ns (b).

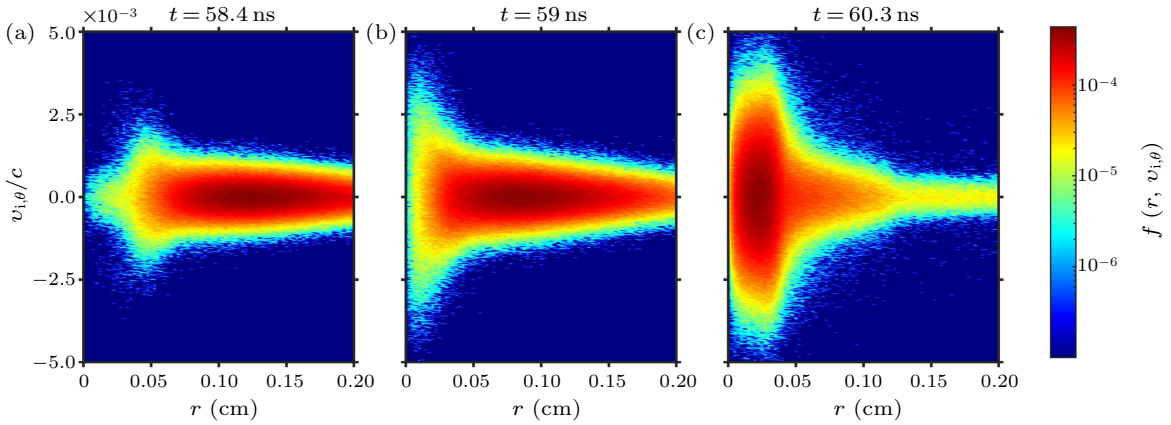


Fig. 7. Diagrams of ion azimuthal-velocity probability distributions in phase space at 58.4 ns (a), 59.0 ns (b), and 60.3 ns (c).

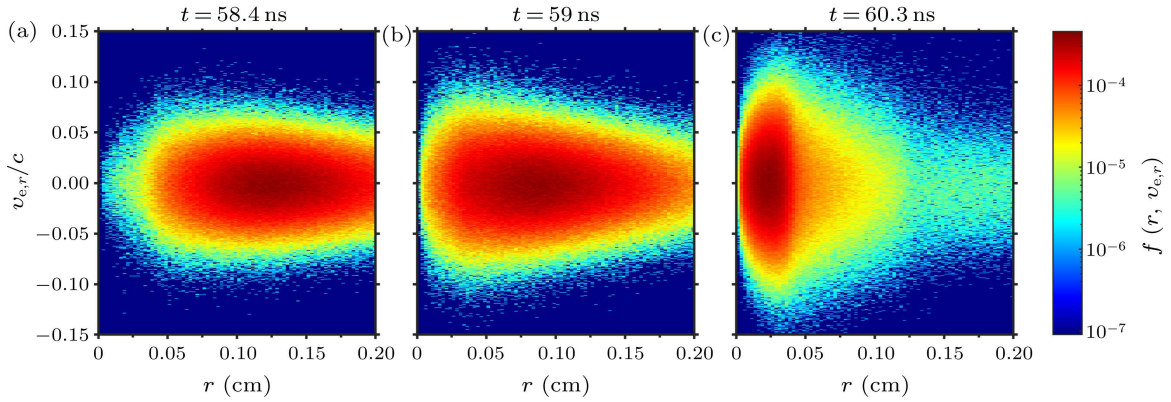


Fig. 8. Diagrams of electron radial-velocity probability distributions in phase space around the stagnation at 58.4 ns (a), 59.0 ns (b), and 60.3 ns (c).

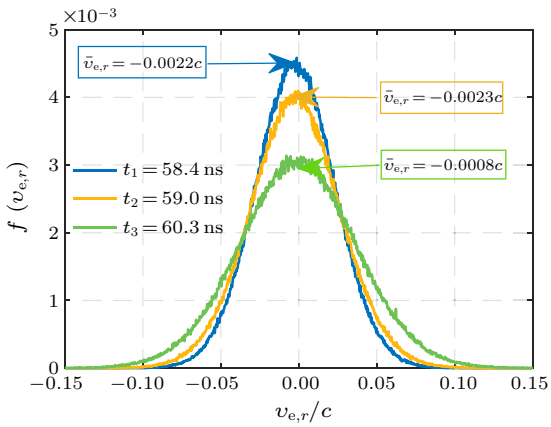


Fig. 9. Radial-velocity probability distributions of electrons at around the stagnation.

3.3. The kinetic characteristic of electron motion

Figures 8(a), 8(b), and 8(c) show the electron radial-velocity probability distributions in v_r–r space at 58.4 ns, 59 ns, and 60.3 ns, respectively. They are equivalent to the phase space diagrams of electron motion at different times. Compared to Figs. 5(b), 5(c), and 5(e) of ion motion phase diagram also at 58.4 ns, 59 ns, and 60.3 ns, respectively, we can be found that there are great differences between them. The main kinetic characteristic of electron motion is oscillation, which should be oscillated around the ions, while that of ion motion is implosion inwards. For well understanding the electron motion status on the whole, the radial-velocity probability distributions of electron are correspondingly presented at around the stagnation in Fig. 9. They are the drift Maxwellian distributions of electron velocity in radius, the electron drift velocity refers to the implosion velocity of electrons. At 58.4 ns, 59 ns, and 60.3 ns, the radial averaged electron velocities $\bar{v}_{e,r}$ are $-2.2 \times 10^{-3}c$, $-2.3 \times 10^{-3}c$, and $-0.8 \times 10^{-4}c$, respectively, which are almost the same as the radial averaged velocities of ions. Moreover, simulation results also indicate that at 60.3 ns there are also differences of $\bar{v}_{e,r}$ in different radial regions, similar to those of ions (see Fig. 6), in the regions of $0 < r < 0.04$ cm and 0.04 cm $< r < 0.2$ cm, $\bar{v}_{e,r}$ are $-4.6 \times 10^{-5}c$ and $-2.0 \times 10^{-3}c$, respectively. However, the electron drift velocities are very small compared to their thermal velocities. The azimuthal and axial electron velocities are Maxwellian distributions, which are consistent with the radial electron distribution due to the strong collisions between electrons. Therefore, based on Eq. (7) and Figs. 5–9, the kinetic picture of Z-pinch can be figured out. The electrons first move inwards under the action of Lorentz force $\boldsymbol{j} \times \boldsymbol{B}$, and then cause separations between electrons and ions for the heavier ion mass. The radial electrostatic fields are produced due to the separations, and in turn the ions are attracted inwards by

the electric force. When the electrons are driven away from ions too much, they will be attracted towards the ions again by the electric force. Thus, the ions are attracted inwards due to the charge separation, and the electrons oscillate around the ions and move inwards with the ions.

3.4. The variations of ion kinetic characteristic with current peaks

From the observation of ion heating, Coulomb collisions play an important role in the energy conversion of ions during stagnation phase. However, if the ion density near the axis region is not sufficiently high, the mean free path of ions (λ_{ii}) may be greater than the stagnation radius (R_{st}).[34,35] This implies that the velocity probability distribution of ions at the axis region might not be the Maxwellian distribution. Therefore, we performed a series of calculations for Z-pinch models with different initial densities, as presented in Table 1, with the same configuration as described at the beginning of this section. The variations in initial density will result in differences in ion density near the axis during the stagnation phase. The current is then determined based on the scaling relationship $I^2 \propto m_l$ where m_l is the linear mass of the Z-pinch load, which is the total mass of the load divided by the length of the load in the z-direction. In Z-pinch, the square of the current is proportional to the magnetic pressure. Therefore, maintaining the proportional relationship between the square of the current and the linear mass ensure that the maximal implosion velocity v_{imp}^{max} keeps consistent in all models. The λ_{ii} in different models can be calculated from the following expression, which is a function of the temperature and density of ions,[36]

$$\lambda_{ii}\,(\mathrm{cm}) = 2.0\times10^{12}[\langle T_{i,st}\rangle\,(\mathrm{eV})]^2/\langle n_{i,st}\rangle\,(\mathrm{cm}^{-3}), \qquad (17)$$

where $\langle T_{i,st}\rangle$ represents the averaged ion temperature at stagnation time, $\langle n_{i,st}\rangle$ represents the averaged ion density within the stagnation radius R_{st} at the stagnation time. To obtain $\langle T_{i,st}\rangle$, we assume that the total kinetic energy of ions was converted into the thermal energy during stagnation phase in all models. Therefore, we can estimate $\langle T_{i,st}\rangle$ by $\langle T_{i,st}\rangle\,(\mathrm{eV}) = m_i(v_{imp}^{max})^2/3|q_e|$, where $v_{imp}^{max} \approx 2.3\times10^{-3}c$. Table 1 displays the ratio of λ_{ii} to stagnation radius in different models.

Figure 10 shows the radial-velocity probability distribution of ions at the stagnation time in all models listed in Table 1. In the case of $I_0 = 0.2$ MA, there are two peaks in the velocity probability distribution, where a peak in the negative direction represents a fraction of ions moving towards the axis, while the other peak in the positive direction does a fraction of ions to be expanding. As I_0 increases in the model settings (meaning an increasing in $\langle n_{i,st}\rangle$), the peaks in the positive and negative directions gradually disappear, and a new peak near the zero velocity appears. This means that the velocity probability distribution gradually transits into a Maxwellian distribution with the current peak increase in a whole. The change in velocity probability distribution is associated with λ_{ii}. As shown in Table 1, when I_0 increases in the model settings, λ_{ii}/R_{st} will continuously decrease. Thus, from model 7 to model 1, it can be inferred that the ions undergo a transition from a collisionless regime to a collisional regime during their stagnation phases. This indicates that only when the peak current is sufficiently high can the plasma achieve a high collision frequency, which facilitates uniform energy distribution and the occurrence of thermonuclear fusion reactions.[21]

Table 1. Peak current I_0, initial density n_0, stagnation time t_{st} (the maximal compression time), stagnation radius R_{st} (the outer radius containing 80% of the plasma mass), and the ratio of ion mean free path to stagnation radius for different models.

Model	I_0 (MA)	n_0 (cm^{-3})	t_{st} (ns)	R_{st} (cm)	λ_{ii}/R_{st}
1	2.00	3.0×10^{18}	60.3	0.050	0.7
2	1.50	1.7×10^{18}	60.2	0.045	1.1
3	1.16	1.0×10^{18}	60.1	0.045	1.9
4	0.80	4.8×10^{17}	60.0	0.050	4.5
5	0.63	3.0×10^{17}	60.0	0.055	7.9
6	0.37	1.0×10^{17}	59.8	0.060	25.7
7	0.20	3.0×10^{16}	59.6	0.069	96.6

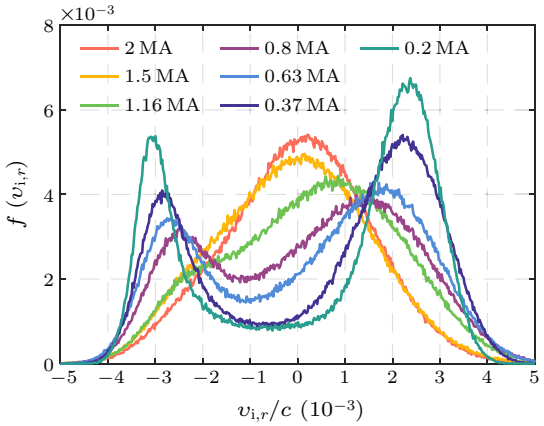


Fig. 10. Radial-velocity probability distributions of ions within R_{st} at stagnation time of all models.

4. Conclusions

For a long time, MHD fluid simulation has been a powerful tool for modeling Z-pinch, with a fundamental assumption that the fluid elements are in thermal equilibrium. In various Z-pinch experiments, the true of this assumption generally holds for electrons, but it may not do for ions. In comparison to MHD fluid simulations, the PIC simulations can provide much more physical details about the ion heating and the velocity probability and temperature distributions of ion and electron in Z-pinch process, especially during the stagnation phase.

In this study, we have developed a novel one-dimensional modified electrostatic implicit PIC algorithm suitable for 1D Z-pinch simulations. This modified electrostatic implicit PIC algorithm is suitable in simulating MHD models with slow

evolution of magnetic fields, while it is easier to implement and has lower computational cost for electromagnetic field solving. In our algorithm, the electromagnetic field solving only accounts for 0.1% of the total program runtime, almost all the runtime is dedicated to the calculations of particle pushing, interpolation, and collisions. The average time spent in per simulation step for field solver, electromagnetic field and particle interpolation, particle pushing, and collisions of the code used in this manuscript and the electromagnetic direct implicit[37] (EMDI) code are shown in Fig. 11. It can be seen that the time spent on solving the electric field in our algorithm is much less than that in the EMDI algorithm. This is because, in our algorithm, the electric field calculation mainly involves solving Poisson's equation. In the EMDI algorithm, one of the major reasons for the larger time spent in solving the electromagnetic fields is the inclusion of time-dependent matrix coefficients in the field equations, which necessitates the use of an iterative solver.[38,39] In Fig. 11, the time spent in interpolation in the EMDI algorithm is larger. This is due to our introduction of the Lapenta matrix[40] in the EMDI algorithm.

Due to the need to use a simplified model for z-direction plasma current calculation in radial one-dimensional algorithms, it may not be very accurate to describe the magnetic field diffusion, thus the differences caused by magnetic field diffusion still need to be carefully considered. However, our simulation practices have shown that our novel Z-pinch PIC simulation method in one dimension is effective.

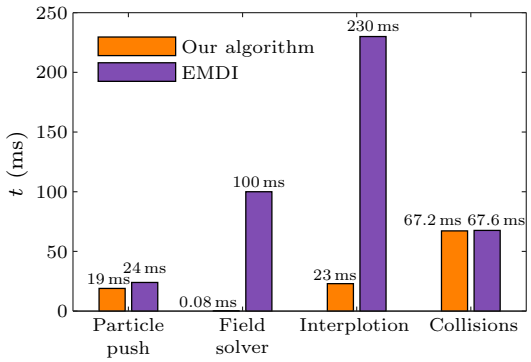


Fig. 11. Average time spent in particle pushing, field solver, electromagnetic field and particle interpolation, and collisions per simulation step.

Based on the 2 MA deuterium plasma shell Z-pinch simulation, the mechanism of ion heating is thoroughly simulated and analyzed. As the ions are approaching to the axis, the main ion heating process occurs when most ions stagnate on the axis, where most ion kinetic energy is converted into thermal energy through stagnation and Coulomb collisions. This results in ion temperatures exceeding 4 keV. Due to the fact that the physically required electron–ion relaxation time is much larger than the duration of the stagnation phase, the temperatures of electrons and ions remain separated. Because of the considerably lower kinetic energy of electrons, the temperature of electron during the stagnation phase is also lower than that of ions. The models with different initial conditions exhibit the significant variations in the radial-velocity probability distribution of ions during the stagnation phase.

Acknowledgments

The authors would like to thank the graduated students Zhixing Feng, Xiaoqiang Zhang, and Deli Fang for their excellent works to develop the PIC simulation codes of Z-pinch. This research was partly supported by the National Natural Science Foundation of China (Grant Nos. 11675025 and 11135007), and the Innovation Project of China Academy of Engineering Physics (Grant No. CX2019030).

References

[1] Spielman R B, Hanson D L, Palmer M A, Matzen M K, Hussey T W and Peek J M 1985 *J. Appl. Phys.* **57** 830
[2] Coverdale C A, Deeney C, Velikovich A L, Clark R W, Chong Y K, Davis J, Chittenden J, Ruiz C L, Cooper G W and Nelson A J 2007 *Phys. Plasmas* **14** 022706
[3] Giuliani J L and Commisso R J 2015 *IEEE Trans. Plasma Sci.* **43** 2385
[4] Spielman R B, Deeney C, Chandler G A, Douglas M R, Fehl D L, Matzen M K, McDaniel D H, Nash T J, Porter J L and Sanford T W L 1998 *Phys. Plasmas* **5** 2105
[5] Deeney C, Douglas M R, Spielman R B, Nash T J, Peterson D L, L'Eplattenier P, Chandler G A, Seamen J F and Struve K W 1998 *Phys. Rev. Lett.* **81** 4883
[6] Slutz S A, Bailey J E, Chandler G A, Bennett G R, Cooper G, Lash J S, Lazier S, Lake P, Lemke R W, Mehlhorn T A, Nash T J, Nielson D S, McGurn J, Moore T C, Ruiz C L, Schroen D G, Torres J, Varnum W and Vesey R A 2003 *Phys. Plasmas* **10** 1875
[7] Ning C and Chen Z 2018 *IEEE Trans. Plasma Sci.* **46** 3794
[8] Wang X, Wang G, Sun S, Xiao D, Ding N, Mao C and Shu X 2022 *Chin. Phys. B* **31** 025203
[9] Maron Y 2020 *Phys. Plasmas* **27** 060901
[10] Klir D, Kubes P, Paduch M, Pisarczyk T, Chodukowski T, Scholz M, Kalinowska Z, Bienkowska B, Karpinski L and Kortanek J 2011 *Plasma Phys. Control. Fusion* **54** 015001
[11] Fan Y, Li Z H, Yi Q, Jiang S Q, Xue F B, Yang J L, Xu R K and Jin Y J 2010 *Chin. Phys. B* **19** 075204
[12] Kroupp E, Osin D, Starobinets A, Fisher V, Bernshtam V, Maron Y, Uschmann I, Förster E, Fisher A and Deeney C 2007 *Phys. Rev. Lett.* **98** 115001
[13] Giuliani J L, Thornhill J W, Kroupp E, Osin D, Maron Y, Dasgupta A, Apruzese J P, Velikovich A L, Chong Y K, Starobinets A, Fisher V, Zarnitsky Yu, Bernshtam V, Fisher A, Mehlhorn T A and Deeney C 2014 *Phys. Plasmas* **21** 031209
[14] Haines M G, LePell P D, Coverdale C A, Jones B, Deeney C and Apruzese J P 2006 *Phys. Rev. Lett.* **96** 075003
[15] Wong K L, Springer P T, Hammer J H, Iglesias C A, Osterheld A L, Foord M E, Bruns H C, Emig J A and Deeney C 1998 *Phys. Rev. Lett.* **80** 2334
[16] Kroupp E, Osin D, Starobinets A, Fisher V, Bernshtam V, Weingarten L, Maron Y, Uschmann I, Förster E, Fisher A, Cuneo M E, Deeney C and Giuliani J L 2011 *Phys. Rev. Lett.* **107** 105001
[17] Baksht R B, Oreshkin V I, Rousskikh A G and Zhigalin A S 2018 *Plasma Phys. Control. Fusion* **60** 035015
[18] Welch D R, Rose D V, Clark R E, Mostrom C B, Stygar W A and Leeper R J 2009 *Phys. Rev. Lett.* **103** 255002
[19] Welch D R, Bennett N, Genoni T C, Rose D V, Thoma C, Miller C and Stygar W A 2019 *Phys. Rev. Accel. Beams* **22** 070401
[20] Angus J R, Link A, Friedman A, Ghosh D and Johnson J D 2022 *J. Comput. Phys.* **456** 111030
[21] Offermann D T, Welch D R, Rose D V, Thoma C, Clark R E, Mostrom C B, Schmidt A E W and Link A J 2016 *Phys. Rev. Lett.* **116** 195001
[22] Welch D R, Rose D V, Thoma C, Clark R E, Mostrom C B, Stygar W A and Leeper R J 2011 *Phys. Plasmas* **18** 056303

[23] Welch D R, Rose D V, Thoma C, Clark R E, Mostrom C B, Stygar W A and Leeper R J 2010 *Phys. Plasmas* **17** 072702
[24] Wang W M, Gibbon P, Sheng Z M and Li Y T 2015 *Phys. Rev. Lett.* **114** 015001
[25] Wang W M, Gibbon P, Sheng Z M and Li Y T 2015 *Phys. Rev. E* **91** 013101
[26] Cohen B I, Langdon A B and Friedman A 1982 *J. Comput. Phys.* **46** 15
[27] Welch D R, Rose D V, Clark R E, Genoni T C and Hughes T P 2004 *Comput. Phys. Commun.* **164** 183
[28] Langdon A B 1979 *J. Comput. Phys.* **30** 202
[29] Nanbu K 1997 *Phys. Rev. E* **55** 4642
[30] Ning C, Sun S K, Xiao D L, Zhang Y, Ding N, Huang J, Xue C and Shu X J 2010 *Phys. Plasmas* **17** 062703
[31] Ning C, Zhang X Q, Zhang Y, Sun S K, Xue C, Feng Z X and Li B W 2018 *Chin. Phys. B* **27** 025207
[32] Mosher D, Weber B V, Moosman B, Commisso R J, Coleman P, Waisman E, Sze H, Song Y, Parks D, Steen P, Levine J, Failor B and Fisher A 2001 *Laser Part. Beams* **19** 579
[33] Takizuka T and Abe H 1977 *J. Comput. Phys.* **25** 205
[34] Angus J R, Link A J and Schmidt A E 2021 *Phys. Plasmas* **28** 010701
[35] Sherlock M, Chittenden J P, Lebedev S V and Haines M G 2004 *Phys. Plasmas* **11** 1609
[36] Ryutov D D 2015 *IEEE Trans. Plasma Sci.* **43** 2363
[37] Welch D R, Rose D V, Clark R E, Genoni T C and Hughes T P 2004 *Comput. Phys. Commun.* **164** 183
[38] Welch D R, Rose D V, Cuneo M E, Campbell R B and Mehlhorn T A 2006 *Phys. Plasmas* **13** 063105
[39] Tan H, Huang T, Ji P, Zhou M, Zhuge L and Wu X 2023 *Chin. Phys. B* **32** 125204
[40] Lapenta G 2017 *J. Comput. Phys.* **334** 349